Int. J. Electrochem. Sci., 5 **(2010)** 1726 - 1742

International Journal of
ELECTROCHEMICAL
SCIENCE
www.electrochemsci.org

Voltammetric and Impedimetric Properties of Nano-scaled γ–Fe_2O_3 Catalysts Supported on Multi-Walled Carbon Nanotubes: Catalytic Detection of Dopamine

Abolanle S. Adekunle[1] *and Kenneth I. Ozoemena*[1,2,*]

[1] Department of Chemistry, University of Pretoria, South Africa.
[2] Energy and Processes Unit, Materials Science and Manufacturing, Council for Scientific and Industrial Research (CSIR), Pretoria 0001, South Africa. Tel.: +27 12 8413664; Fax: +27 12 8412135
[*]E-mail: kozoemena@csir.co.za

Received: 31 August 2010 / *Accepted:* 15 September 2010 / *Published:* 1 December 2010

The electron transfer and electrocatalytic proiperties of iron oxide nanoparticle (γ-Fe_2O_3) catalysts supported on MWCNTs are described. The MWCNT-Fe_2O_3 and its electrodes were successfully characterised with FESEM, HRTEM, XRD, EDX, cyclic voltammetry and electrochemical impedance spectroscopy. The MWCNT-Fe_2O_3 based electrodes demonstrated fastest electron transport and current response towards DA compared to other electrodes studied, giving a catalytic rate constant of 16.4 x 10^5 $cm^3mol^{-1}s^{-1}$, sensitivity of 0.026 AM^{-1} and limit of detection of 3.3 x 10^{-7} M. The electrode may be potentially useful for the detection of DA in real drug sample analysis.

Keywords: MWCNTs, iron oxide nanoparticles, voltammetry, electrochemical impedance spectroscopy, dopamine detection

1. INTRODUCTION

Applications of nanosized magnetic particles have received considerable attention in biotechnology and medicine for their novel properties [1,2]. Iron is a versatile element and can form several phases with different oxidation states and structures such as shown below [3].

$$FeO \leftrightarrow FeO \leftrightarrow Fe_3O_4 \leftrightarrow \gamma\text{-}Fe_2O_3 \leftrightarrow \alpha\text{-}Fe_2O_3 \leftrightarrow FeOOH \qquad (1)$$

Magnetite (Fe_3O_4), maghemite (γ-Fe_2O_3), and hematite (α-Fe_2O_3) are probably the most common out of the many oxides form in which iron oxides exist in nature [4]. The use of iron and its complexes in sensing is well established [5-8].

Carbon nanotubes (CNTs) have attracted numerous experimental and theoretical investigations due to its exciting structural stability, mechanical and electronic properties [9,10]. Several authors have reported the excellent electrocatalytic properties of nanotubes in the redox behaviour of different molecules and bio-molecules [11-18]. Thus carbon nanotubes-modified electrodes have shown interesting catalytic properties during electrochemical processes. Dopamine (DA) is one of the most significant catecholamines and belongs to the family of excitatory chemical neurotransmitters [19]. It plays a very important role in the functioning of the central nervous, cardiovascular, renal, and hormonal systems, as well as in drug addiction and Parkinson's disease [20,21]. It has also been reported that DA system dysfunction plays a critical role in some clinical manifestations of HIV infection [22]. Thus, it becomes imperative and challenging for neuro and analytical scientist to fabricating a sensor that will determine the presence of this molecule in its trace amount in human fluid. In recent times, electrochemical techniques have been used to investigate the role of neurotransmitters in the brain due to their electroactive nature [23].

In this study, we report the voltammetric detection of dopamine using easily prepared nano-scaled iron oxide (Fe_2O_3) catalyst supported on multi-walled carbon nanotubes (MWCNT) modified pyrolytic graphite electrode. The detection of dopamine using electrochemically formed Fe_2O_3 nanoparticles supported on single-walled carbon naotubes (SWCNTs) was recently reported. Thus, some of the motivating factors for embarking on this particular study include (i) the ability to produce nano-scaled iron oxides in high commercial quantity compared to the very low and commercially unavailable amount inherent with the electrodeposition method, (ii) low or non-passivation of the electrode modified with laboratory-synthesised Fe_2O_3 nanoparticles compared with their electrodeposited counterparts, and (iii) commercial availability of MWCNTs over the SWCNTs in terms of cost implication

2.EXPERIMENTAL PART

2.1. Materials and Reagents

Multi-walled carbon nanotubes (MWCNTs), obtained from Aldrich, was acid-digested using the known procedure [24]. $Fe(NO_3).9H_2O$ was obtained from Sigma-Aldrich chemicals. $NH_3.H_2O$ solution, $NaBH_4$, Na_2SO_3, HCl and ethanol were obtained from Merck chemicals. Dopamine drug (Dopamine HCl-Fresenius® (200 mg / 5 ml) product of Bodene (pty) Ltd South Africa, was supplied by a local pharmacy store. Ultra pure water of resistivity 18.2 MΩcm was obtained from a Milli-Q Water System (Millipore Corp., Bedford, MA, USA) and was used throughout for the preparation of solutions. Phosphate buffer solutions (PBS) at various pHs were prepared with appropriate amounts of K_2HPO_4 and KH_2PO_4, and the pH adjusted with 0.1 M H_3PO_4 or NaOH. All electrochemical

experiments were performed with nitrogen-saturated PBS. All other reagents were of analytical grades and were used as received from the suppliers without further purification.

2.1.1. Synthesis of iron and iron oxide nanoparticles

Nanoscale zero-valent iron (Fe^0) particles were synthesized by the sodium borohydride method as described by Sun *et al*. [25]. The synthesis was conducted in a flask reactor with three open necks. The central neck was housed with a tunable mechanical stirrer at 400 rpm. 50 mL (0.2 M) $NaBH_4$ was titrated slowly into 50 mL (0.05 M) $Fe(NO_3).9H_2O$ solution. The borohydride was introduced to reduce ferric ion (Fe^{3+}) to zero-valent iron [Fe^0], according to the following reaction:

$$4Fe^{3+} + 3BH_4^- + 9H_2O \longrightarrow 4Fe^0 + 3H_2BO_3^- + 12H^+ + 6H_2 \quad (2)$$

The mixture was vigorously mixed in the flask reactor for additional 30 min after the titration. The generated iron particles were harvested with vacuum filtration and stabilized with a large volume of deionized water (>100 mL/g) to wash, and at the end, with diluted ethanol (~5%).

The maghemite (Fe_2O_3) nanoparticles were synthesized by the method described elsewhere [26]. First, Magnetite (Fe_3O_4) nanoparticles were synthesized according to the method proposed by Qu et al. [27] but with some modification. Briefly, 9 mL (2 M) $Fe(NO_3).9H_2O$ (dissolved in 2 M HCl) was added to 300 mL double-distilled water, and 10 mL Na_2SO_3 (1 M) was added to the former solution drop wise in 1 min under magnetic stirring. The colour of the solution changed from light yellow to red, indicating complex ions formed between the Fe^{3+} and SO_3^{2-}. When the color of the solution turned back again, the solution was added to 300 mL $NH_3.H_2O$ solution (0.85 M) under vigorous stirring. A black precipitate is formed and allowed to crystallize completely for about an hour under magnetic stirring. The precipitate was washed with copious amount of water to bring the pH of the suspension to less than 7.5. The suspension was dried into black powder at ambient temperature under vacuum. The black precipitate obtained above was diluted to a volume of 300 mL. The suspension temperature was raised to 90 ^oC in 5 min, and was stirred under aeration for 60 min at about 100 ^oC. A colour changed from black to reddish-brown slowly while the suspension became clear and transparent. The reddish-brown solution was washed with water by magnetic decantation four times. It was then dried to powder in the oven at 70 ^oC.

2.2. Equipment and Procedure

The edge plane pyrolytic graphite (EPPG) plate was purchased from Le Carbone, Sussex, UK and was constructed locally by placing it in a teflon tube, extended outside with a copper wire to make electrical contact with the electrochemical equipment. High resolution scanning electron microscopy (HRSEM) image was obtained using the Zeiss Ultra Plus 55 HRSEM (Germany), while the energy dispersive x-ray spectra (EDX) were obtained from NORAN VANTAGE (USA). Transmission electron microscopy (TEM) experiment was performed using a Model JEOL JEM-2100F field emission transmission electron microscope, Tokyo (Japan). The XRD analysis was done using a back

loading preparation method. The sample was analysed using a PANalytical X'Pert Pro powder diffractometer (Netherland) with X'Celerator detector and variable divergence- and receiving slits with Fe filtered Co-Kα radiation.

Electrochemical experiments were carried out using an Autolab Potentiostat PGSTAT 302 (Eco-Chemie, Utrecht, and The Netherlands) driven by the GPES software version 4.9. Electrochemical impedance spectroscopy (EIS) measurements were performed with Autolab Frequency Response Analyser (FRA) software between 10 mHz and 10 kHz using a 5 mV rms sinusoidal modulation. A Ag|AgCl, sat'd KCl (3M) and platinum wire were used as reference and counter electrodes, respectively. The unmodified and modified EPPGE served as the working electrodes. All solutions were de-aerated by bubbling nitrogen prior to each electrochemical experiment. All experiments were performed at 25±1 °C.

2.2.1. Preparation of the dopamine hydrochloride injection solution

A 2 mL of the drug (dopamine hydrochloride injection- Dopamine HCl-Fresenius®) sample was diluted to 100 mL with distilled de-ionised water. 2 mL of the diluted solution was pipette into each of 50 mL volumetric flask and all except one were spiked with different concentration of standard dopamine solution, and made to volume with phosphate buffer pH 7.0. The concentration of each test aliquot solution was determined using square wave voltammetry. Four different injections from the same batch were analysed using the same procedure. The experiment was repeated 5 times for each sample.

2.3. Electrode Modification and Pre-treatments

EPPGE surface was cleaned by gentle polishing in aqueous slurry of alumina nanopowder (Sigma-Aldrich) on a SiC-emery paper and then to a mirror finish on a Buehler felt pad. The electrode was then subjected to ultrasonic vibration in absolute ethanol to remove residual alumina particles that might have been trapped at the surface. EPPGE-MWCNT was prepared by a drop-dry method. Different weights (2.5 to 10 mg) of the synthesised Fe and Fe_2O_3 nanoaparticles were weighed and dissolved in dimethylformamide (DMF) along with and without 2 mg of the functionalised MWCNTs. The mixture was stirred at room temperature for 48 h. About 20 µL of the MWCNT-Fe or MWCNT-Fe_2O_3 was drop-cast on the EPPGE and annealed in the oven at 50^0 C for 5 min. The modified electrode is denoted as EPPGE-MWCNT-Fe or the EPPGE-MWCNT-Fe_2O_3. Other electrodes were obtained using similar procedure

3. RESULTS AND DISCUSSION

3.1. Comparative TEM, HRSEM, EDX and XRD spectra.

Figure 1 is the typical TEM micrograph for the MWCNT-Fe (a) and the MWCNT-Fe_2O_3 (b). Their corresponding HRSEM images are represented in Figure 1c and d respectively. All the

micrographs showed very high dispersion of Fe and Fe_2O_3 nanoparticles along the MWCNTs which is made possible because of the strong electrostatic interactions between the Fe^{2+} or Fe^{2+} ions in solution and the COO^- charge of the MWCNTs. From the TEM, a representative single particle size is around 20-50 nm for Fe and 5-13 nm for Fe_2O_3 which agreed closely with 60-70 nm reported for Fe [25], and 8.6 nm for γ-Fe_2O_3 nanoparticles [26].

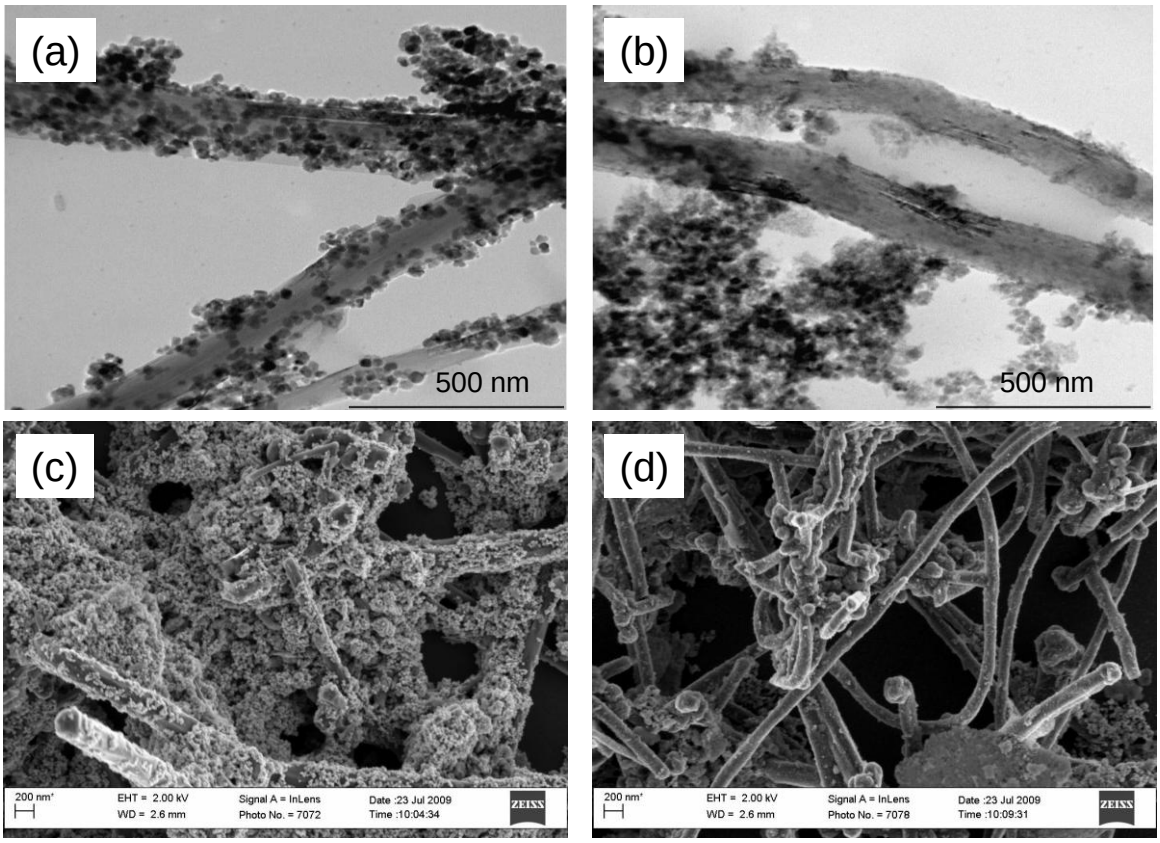

Figure 1. TEM images of (a) MWCNT-Fe (b) MWCNT-Fe_2O_3. (c) and (d) HRSEM picture of MWCNT-Fe and MWCNT- Fe_2O_3 respectively.

The XRD spectra for the nanosized particles are shown in Figure 2. Characteristic peaks at 2θ of 21.3, 35.2, 41.5, 50.6, 62.6, 67.4 and 74.3, which are indexed as (111), (220), (311), (400), (422), (511) and (440) were observed. The result agreed with that observed by others [26,28] indicating that the resultant particles were cubic spinel structure for γ-Fe_2O_3. From Debye-Scherrer equation [26]:

$$d = \frac{K\lambda}{B\cos\theta} \tag{3}$$

where d is the average crystal size; K is a constant (0.89); λ is the wavelength (1.78901 nm) used; B is the full width at half maximum of the peak, θ is the Bragg's angle of the XRD peak, the crystal size of the Fe_2O_3 particles were estimated from the peaks to be ~ 10.3 nm, which falls in the range shown by the TEM. Inset in Figure 2 is the XRD spectrum of the Fe nanoparticles. Apparent

peaks at 2θ of 41.8 and 35.4 indicate the presence of both zero-valent iron (Fe) and iron oxide (FeO) [25]. Traces of FeO particles not completely reduced to Fe were also confirmed by the presence of trace oxygen peak in the EDX profile (see Fig 3a).

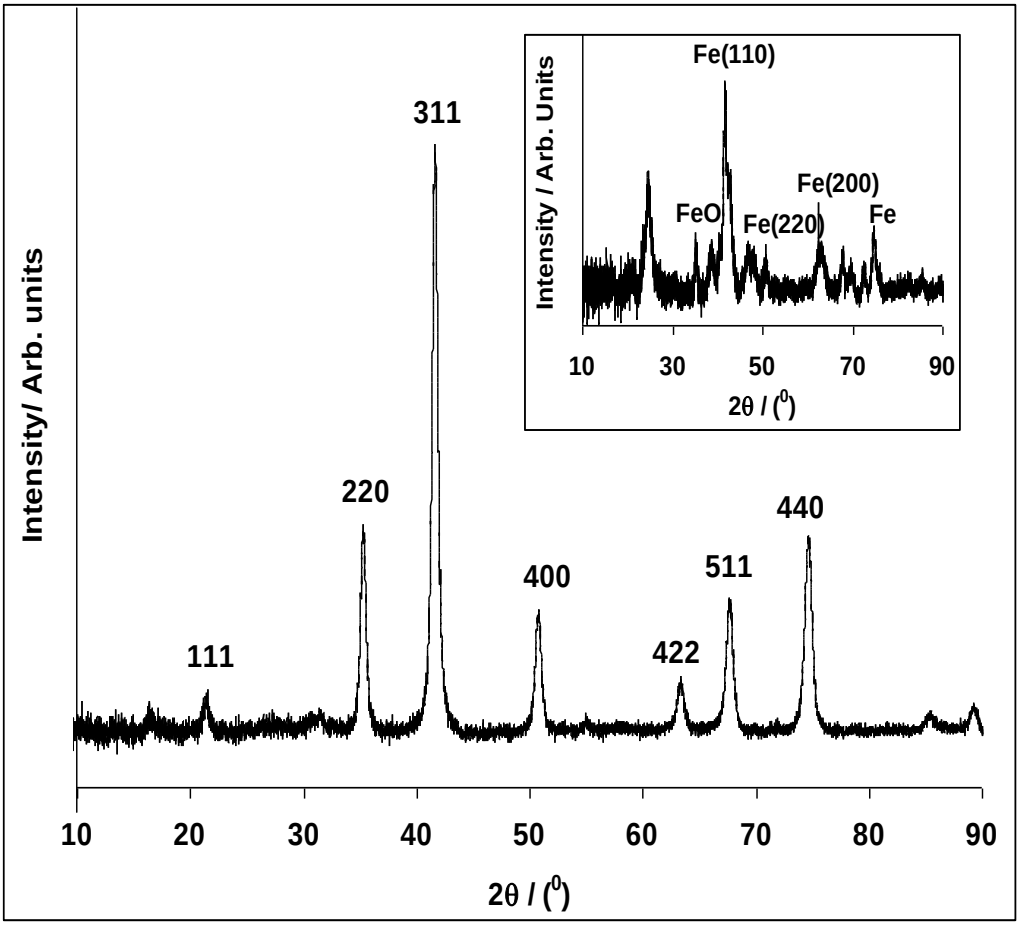

Figure 2: XRD spectrum of Fe_2O_3 nanoparticles. Inset is the XRD spectrum of Fe nanoparticles.

Figure 3 are the EDX profile of the synthesised MWCNT-Fe (a) and MWCNT-Fe_2O_3 (b). The carbon peak in both is attributed to the carbon of the MWCNT or the base carbon coating for enhancing the conductivity of the material. The presence of Fe peaks in both (a) and (b) compared with other elements also confirm the successful modification of the MWCNTs with Fe or Fe_2O_3 nanoparticles. Presence of O peak in (b) is linked with traces of unreduced iron oxide and the oxo-functionalities of the functionalised MWCNTs. The sulphur peak can be attributed to the sulphuric acid used during MWCNT treatment.

3.3 Comparative electron transfer properties

Figure 4 is the comparative cyclic voltammograms of the electodes in 5 mM $Fe(CN)_6]^{4-}$ /$[Fe(CN)_6]^{3-}$ solution. The redox couple in the 0.0 – 0.4 V regions (**II**) is due to the $Fe(CN)_6]^{4-}$

/$[Fe(CN)_6]^{3-}$ redox process. This couple is absent in 0.1 M PBS (pH 7) alone. The broad redox process in the -0.2 – 0.2 V region (**I**) is ascribed to the Fe^{3+}/Fe^{2+} of the iron or iron oxide, presumably the γ-Fe_2O_3 / Fe_3O_4. The poorly defined redox couples in the 0.5 – 0.7 V (**III**) is presumably due to the redox process involving the α-phase (i.e., α-Fe_2O_3 / FeOOH).

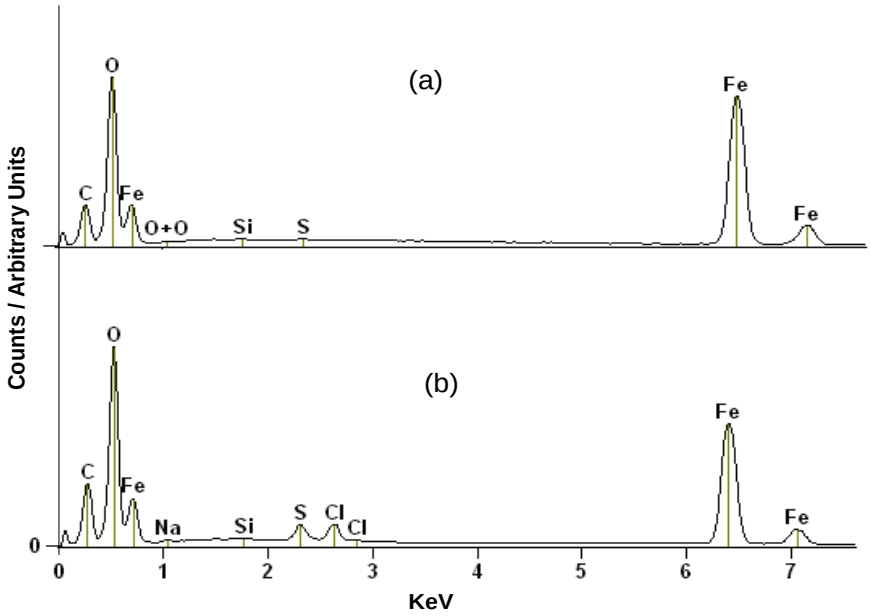

Figure 3. EDX profiles of MWCNT-Fe and MWCNT-Fe_2O_3 respectively.

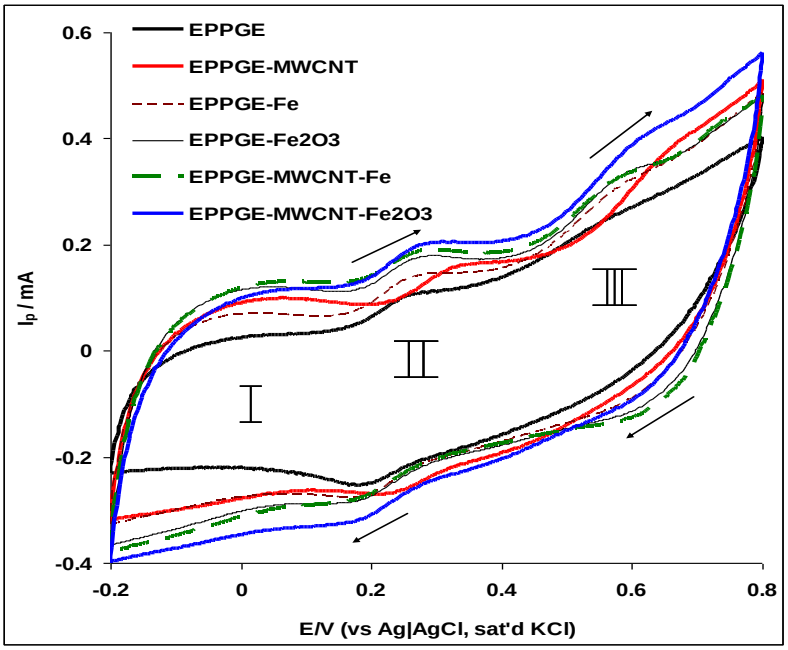

Figure 4. Comparative cyclic voltammetric evolutions of the electrodes in 5 mM $[Fe(CN)_6]^{4-}$ /$[Fe(CN)_6]^{3-}$ in pH 7.0 PBS (scan rate = 50 mVs^{-1})

Further study to understand the electronic transport properties of the modified electrodes was carried out using electrochemical impedance spectroscopic (EIS) technique (biased at 0.2 V, the equilibrium potential, $E_{1/2}$, of the $[Fe(CN)_6]^{4-}/[Fe(CN)_6]^{3-}$ couple). The Nyquist plot obtained (Fig. 5a) was satisfactorily fitted using the electrical equivalent circuit model shown in Figure 5b. The circuit parameters consist of a constant phase element (CPE), electrolyte resistance (R_s), charge-transfer resistance (R_{ct}) and the double layer capacitance C_{dl}. From the R_{ct} value values (Table 1), the electron-transport is faster at the EPPGE-MWCNT-Fe and EPPGE-MWCNT-Fe_2O_3 electrodes (R_{ct} ~ 20.0 Ωcm^2) compared to others. The n values close to the ideal Warburg diffusive value of 0.5, is indicative of some diffusion process at the electrode.

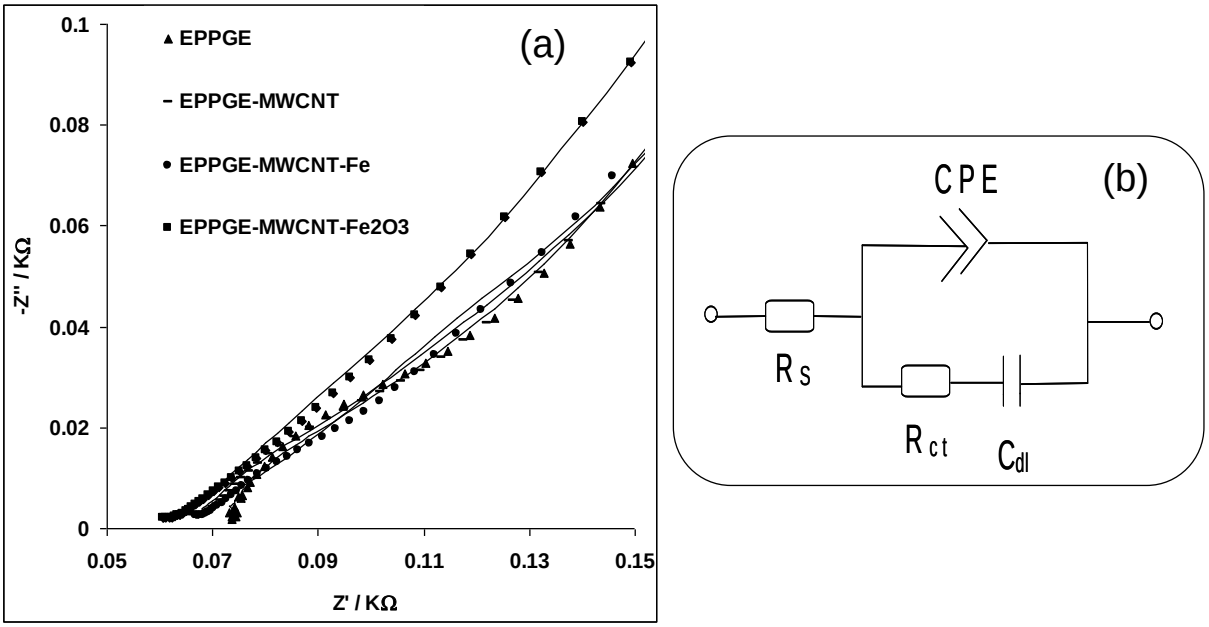

Figure 5. (a) Typical Nyquist plots obtained for some of the electrodes in 5 mM $[Fe(CN)_6]^{4-}$ / $[Fe(CN)_6]^{3-}$ solution at a fixed potential of 0.2 V (vs Ag|AgCl, sat'd KCl). The data points are experimental while the solid lines in the spectra represent non-linear squares fits. (b) is the circuit used in the fitting of the EIS data in (a).

3.4. Comparative electrocatalytic oxidation of dopamine

Figure 6 is the comparative cyclic voltammograms of the electrodes in 0.1 M PBS containing $2x10^{-4}$ M dopamine (DA). DA catalysis was studied at different loading (2.5 – 10 mg mL^{-1}) of Fe and Fe_2O_3 nanoparticles or their nanocomposite with MWCNT on the electrode. Since Fe, Fe_2O_3 and the MWCNTs are characterised with background (or capacitive) current, the current due to dopamine electro-oxidation (*ca* 0.2 V) on the electrodes was obtained after the background subtraction. Interestingly, when compared to all known literature reports on dopamine oxidation at modified electrodes, to our knowledge, this represents the first time two pairs of redox couples are observed for dopamine. From the preceding discussion, the first DA redox couple (Dopamine / Quinone) at $E_{1/2}$ of 0.16 V is the usual mediated by the Fe^{3+}/Fe^{2+} (i.e., the γ-Fe_2O_3 / Fe_3O_4). The second redox couple at

$E_{1/2}$ of 0.40 V is the same Dopamine / Quinone, which is now presumably mediated by the α-phase (i.e., α-Fe_2O_3 / FeOOH). The highest DA signal was obtained at 5.0 mg/ml loading of the nanocomposite on the electrode and the trend in current response follows as: MWCNT-Fe_2O_3 >> MWCNT-Fe > MWCNT > EPPGE ≈ Fe_2O_3 > Fe. The current response at the MWCNT-Fe_2O_3 electrode is about two times higher than that at the bare electrode as well as the electrodes based on MWCNT or Fe nanoparticles alone.

Table 1. Impedance data obtained for the bare and the modified EPPGE electrodes in 5 mM $Fe(CN)_6]^{4-}$/$[Fe(CN)_6]^{3-}$ solution at 0.2 V (vs Ag|AgCl sat'd KCl). All values were obtained from the fitted impedance spectra after several iterations using the circuits.

Electrodes	Impedimetric parameters				
	R /Ωcm^2	Q /μFcm^{-2}	n	R /Ωcm^2	C_{dl} / mFcm^{-2}
EPPGE	6.96±0.01	14.0±1.24	0.51±0.01	35.00±0.19	1.28±0.06
EPPGE-MWCNT	6.46±0.01	11.3±1.16	0.49±0.01	35.30±0.20	1.72±0.08
EPPGE-Fe	3.14±0.01	10.8±1.01	0.47±0.01	24.15±0.13	3.10±0.15
EPPGE-Fe_2O_3	3.29±0.01	161.8±19.61	0.55±0.01	27.10±0.69	1.15±0.22
EPPGE-MWCNT-Fe	3.33±0.01	38.0±4.74	0.49±0.01	20.2±0.18	3.94±0.30
EPPGE-MWCNT-Fe_2O_3	3.08±0.01	91.8±8.18	0.52±0.01	19.75±2.05	2.78±0.23

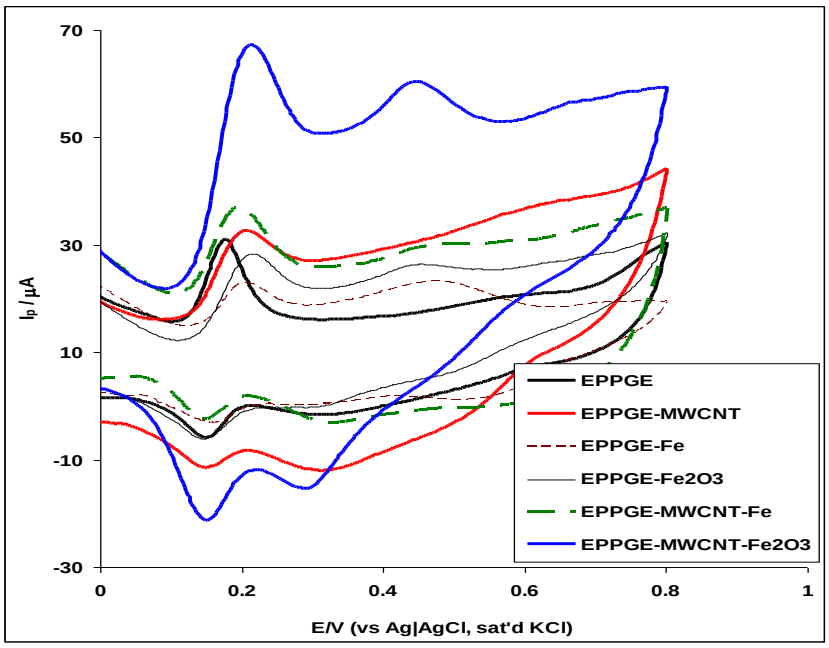

Figure 6. Comparative current response (after background current subtraction) of the electrodes: (i) EPPGE, (ii) EPPGE-MWCNT, (iii) EPPGE-Fe, (iv) EPPGE-Fe_2O_3, (v) EPPGE-MWCNT-Fe, and (vi) EPPGE-MWCNT-Fe_2O_3 in 2x10^{-4} M DA solution in pH 7.0 PBS (scan rate = 25 mVs^{-1}).

The DA oxidation current decreased with increasing loading (7.5 to 10 mg/mL) of the nanocomposite suggesting electrode layer passivation. The enhanced DA response at EPPGE-MWCNT-Fe_2O_3 may be ascribed to either (1) facile interaction of MWCNTs and Fe_2O_3, or (2) the ease of diffusion of DA through the MWCNT-Fe_2O_3 film to the electrode surface, or (3) the ability of the iron (III) to forms a chelate with the dihydroxy catechol group of dopamine, catechol, 5, 6-dihydroxyindole [29], or all of them. The DA current response at the MWCNT-Fe_2O_3 films modified electrode is also higher compared with 50.45 μA reported for the SWCNT-Fe_2O_3 electrode prepared by electrodeposition method [30]. The result therefore suggest that the synthetic method adopted in this study could be a better approach for electrode modification with the nanocomposite materials in large quantity, and at lesser cost for commercial application in sensor and other electrochemical devices. Therefore, all other studies carried out in this work, unless otherwise stated, were carried out using EPPGE-MWCNT-Fe_2O_3 electrode.

Effect of scan rate (ν) was investigated by carrying out cyclic voltammetry experiment at constant concentration (2 x 10^{-4} M) of DA in 0.1 M PBS using the EPPGE-MWCNT-Fe_2O_3 electrode (Fig. 7).

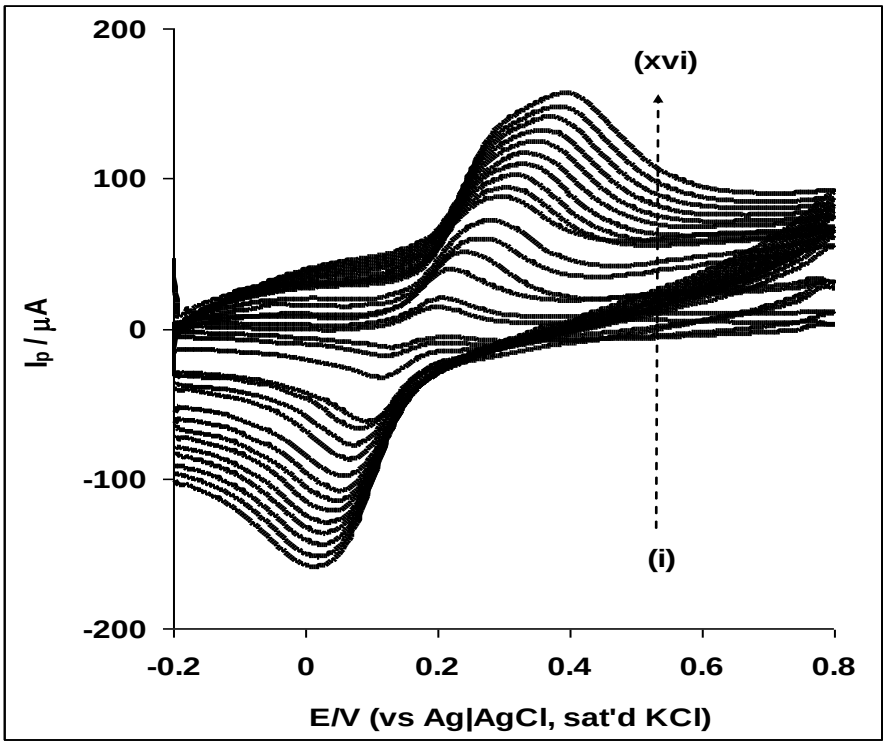

Figure 7. Cyclic voltammetric evolutions of EPPGE-MWCNT-Fe_2O_3 obtained in 0.1 M PBS containing 2 x 10^{-4} M DA (scan rate range 25 – 1000 mVs^{-1}; inner to outer).

It was observed that DA anodic and cathodic peaks increase simultaneously with increase in scan rates (25–1000 mV s^{-1}). A pair of well defined symmetrical redox peaks (I_{pa} /I_{pc} ~ 1.0), even at high scan rates was observed. However, plots of the anodic (I_{pa}) against the square root of scan rate

($\nu^{1/2}$) (not shown) for the scan rate range studied gave a linear relationship with scan rates (R^2 = 0.9932), suggesting a diffusion-controlled redox process.

Electro-oxidation of DA at the electrodes was investigated using EIS at a fixed potential (0.2 V vs. Ag|AgCl, sat'd KCl) and frequency range of 10 kHz to 10 mHz. Figure 8 represents the Nyquist plots obtained for some of the electrodes. Inset is the modified Randles circuit model used in the fitting of the experimental data. The circuit elements consist of a constant phase element (CPE), electrolyte resistance (R_s), charge-transfer resistance (R_{ct}) and the double layer capacitance C_{dl}. The R_{ct} value (31.6 Ωcm^2) for EPPGE-MWCNT-Fe_2O_3 is relatively low compared with the 33.4 Ωcm^2 for bare EPPGE and 38.9 Ωcm^2 for EPPGE-MWCNT (Table 2). The results demonstrated the role of the MWCNT in forming a synergy with the Fe_2O_3 nanoparticles in improving the catalysis and electron transport of the MWCNT-Fe_2O_3 electrode towards DA oxidation. Presently, there is very little information on DA electrochemical impedance study. The information using a fibre (SiC-C) electrode for DA sensing [31] indicated that the electrode showed a capacitive behaviour which, according to the authors, is highly desirable for chemical and electrochemical stability of the electrodes.

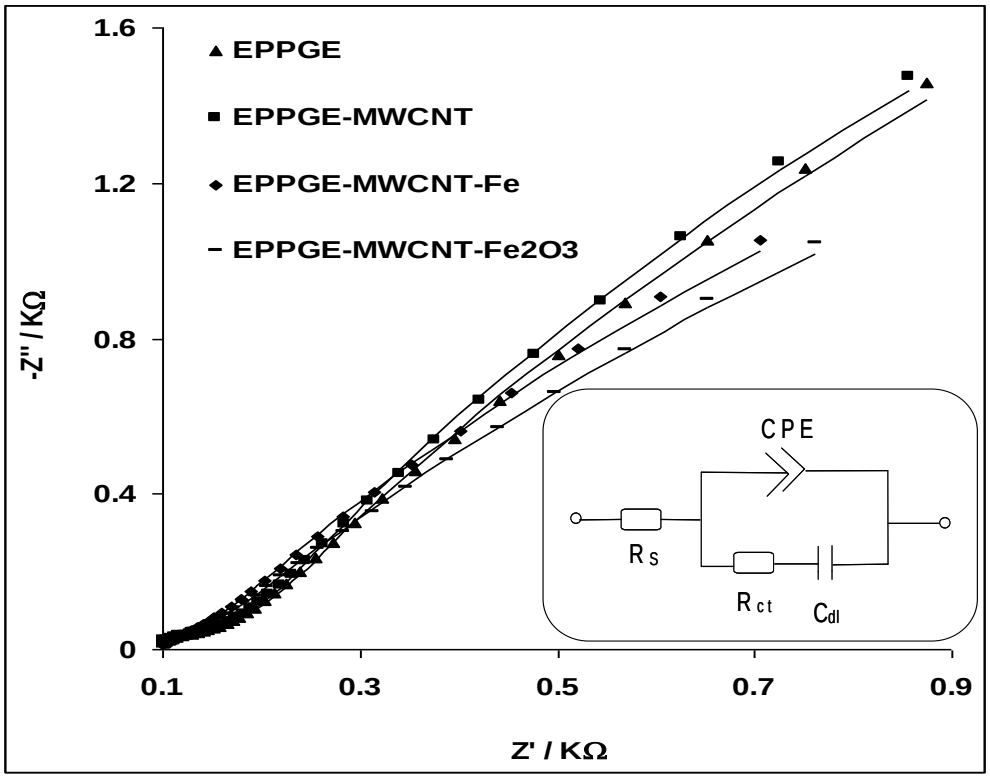

Figure 8. Typical Nyquist plots obtained for some of the electrodes in 2 x 10^{-4} M DA solution at a fixed potential of 0.2 V. Inset is the Randles circuit model used in fitting the data.

The stability of the electrode was studied by continuous scanning in 2×10^{-4} M DA at 25 mVs^{-1}. About 40% current decrease was observed after the first scan which could be due to the adsorbed species on the electrode. However, on rinsing the electrode in a fresh PBS (pH 7.0) solution, the electrode surface

became renewed and a current increase (> 90%) of the initial catalytic current was obtained. The result therefore suggests that the electrode is electrochemically stable and can be reused after an experiment. The electrode also demonstrated an insignificant change to DA current response during DA analysis after storage in a refrigerator for up to two weeks.

Table 2. Impedance data obtained for the bare and the modified EPPGE electrodes in 2 x 10^{-4} M DA in pH 7.0 PBS at 0.2 V (vs Ag|AgCl sat'd KCl). All values were obtained from the fitted impedance spectra after several iterations using the circuits.

Electrodes	Impedimetric parameters				
	$R_s/\Omega cm^2$	$Q/\mu Fcm^{-2}$	n	$R_{ct}/\Omega cm^2$	$C/ mFcm^{-2}$
EPPGE	8.32±0.01	24.19±2.15	0.57±0.01	33.40±0.13	2.20±0.05
EPPGE-MWCNT	8.30±0.01	25.06±2.09	0.58±0.01	38.90±0.16	2.19±0.08
EPPGE-Fe	8.71±0.01	12.39±1.27	0.53±0.01	40.30±0.17	2.40±0.09
EPPGE-Fe_2O_3	8.71±0.01	96.23±4.86	0.61±0.01	57.50±0.36	1.40±0.07
EPPGE-MWCNT-Fe	8.77±0.01	133.50±12.88	0.62±0.01	30.85±0.31	1.67±0.12
EPPGE-MWCNT-Fe_2O_3	8.42±0.01	83.06±4.86	0.59±0.01	31.60±0.21	1.46±0.07

3.5. Analytical application

Concentration study was carried out by investigating the response of EPPGE-MWCNT-Fe_2O_3 electrode to the different concentrations of DA (Fig. 9) using square wave voltammetry (SWV) experiments at a fixed potential of 0.20 V. From the plot of current response against concentration (not shown), a linear relationship was obtained for concentration range of 6.3 to 25.0 µM. The sensitivity was calculated as 0.026±0.002 $\mu A \mu M^{-1}$, while the limit of detection (LoD = 3.3 s/m [32], where *s* is the relative standard deviation of the intercept and *m*, the slope of the linear current versus the concentration of DA) was 3.3 x 10^{-7} M. The limit of detection obtained in this study agreed closely with the 0.36 µM reported for EPPGE-SWCNT-Fe_2O_3 using same technique [30] but much lower, or at about the same magnitude with values reported in literature for DA electro-oxidation [33-40].

The catalytic rate constant (*k*) for the oxidation of DA at the EPPGE-SWCNT-Fe_2O_3 electrode was estimated using chronoamperomatric technique from the relationship [41,42] (equation 4):

$$\frac{I_{cat}}{I_{buff}} = \pi^{1/2}(kCt)^{1/2} \quad (4)$$

where I_{cat} and I_{buff} are the currents in the presence and absence of DA, respectively; k is the catalytic rate constant and t is the time in seconds. From the slope of the plots of I_{cat}/I_{buff} vs. $t^{1/2}$ at different DA concentrations (not shown), the k value was estimated as 16.4 x 10^5 cm^3 mol^{-1} s^{-1}. The k value is greater compared with 4.67 x 10^5 cm^3 mol^{-1} s^{-1} reported for DA on aluminium electrode modified with palladium hexacyanoferate (PdHCF) films [43] and 3.1 x 10^5 $cm^3mol^{-1}s^{-1}$ on aluminium electrode modified with nickel pentacyanonitrosylferrate (NiPCNF) film [44]. The diffusion coefficient D for DA at the electrode was estimated from the Cottrell Equation (5) below [45]:

$$I = \frac{nFAD^{1/2}C}{\pi^{1/2}t^{1/2}} \quad (5)$$

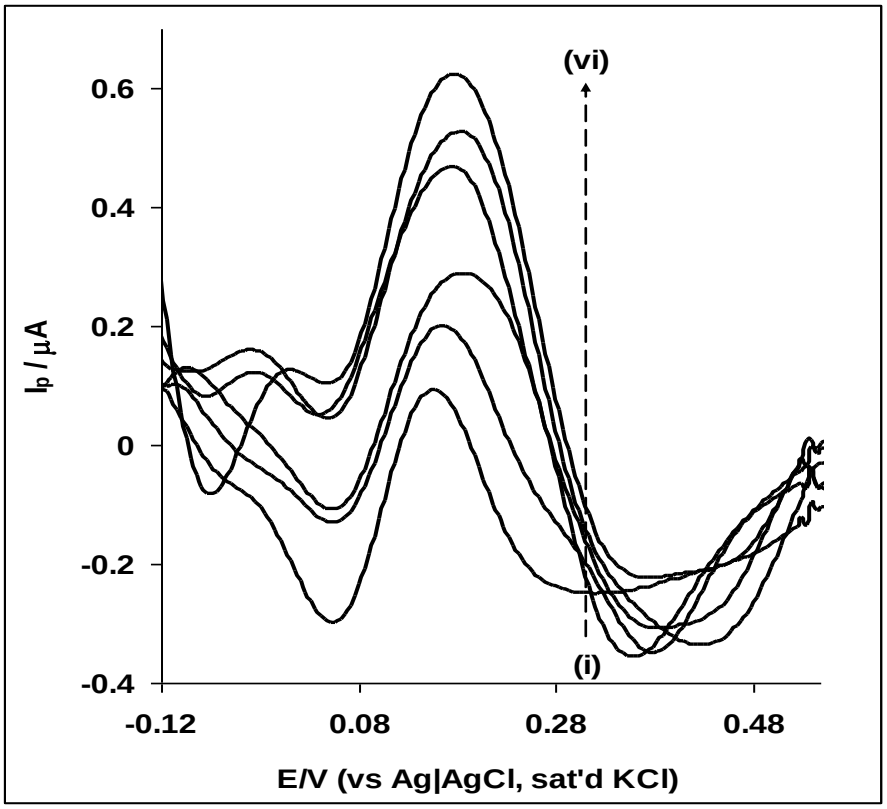

Figure 9. Square wave voltammetric evolutions of the EPPGE-MWCNT-Fe_2O_3 in 0.1 M PBS pH 7.0 containing different concentration of DA (6.25, 11.8, 14.7, 21.1, 23.1 and 27.0 µM).

where C is the bulk concentration (mol cm^{-3}), A is the area of the electrode in cm^2 and assuming n ≈ 2, the diffusion coefficient D for DA was calculated from the slope of the experimental

plots of I versus $t^{-1/2}$ (not shown), as 8.4 x 10^{-5} cm^2 s^{-1}. The D value is a magnitude higher than the 2.5 x 10^{-6} cm^2 s^{-1} reported for DA on aluminium electrode modified with palladium hexacyanoferate (PdHCF) films [43], and 3.4 x 10^{-6} cm^2 s^{-1} for DA on aluminium electrode modified with nickel pentacyanonitrosylferrate (NiPCNF) film [44]. The difference in K and D reported for the electrodes is due to their different surface electroactive materials.

3.6. Interference study

Figure 10 shows the square wave voltammetric responses of AA in the absence (i) 1 mM AA alone, and mixture of (ii) 4.76 µM DA and 0.95 mM AA, (iii) 9.09 µM DA and 0.91 mM AA, (iv) 13.04 µM DA and 0.87 mM AA, (v) 20.0 µM DA and 0.8 mM AA, (vi) 25.93 µM DA and 0.74 mM AA and (vii) 28.57 µM DA and 0.71 mM AA in PBS pH 7.0 at the EPPGE-MWCNT-Fe_2O_3 electrode. In the presence of DA, AA signal was seen at about 0.18 V and DA at around 0.37 V on the electrode, which is contrary to AA and DA position observed at *ca* 0.1 and 0.2 V respectively on our previously reported EPPGE-SWCNT-Fe_2O_3 electrode made by electrodeposition [30]. Cao et al. [46] also observed AA and DA signal at 0.14 and 0.43 V respectively on CPB/chitosan composite films modified glassy carbon electrode.

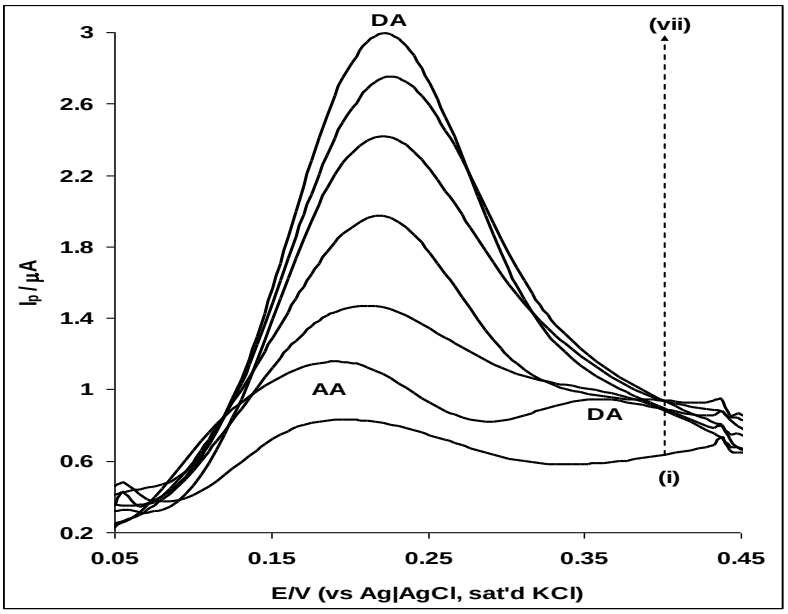

Figure 10. Typical square wave voltammograms responses of EPPGE-MWCNT-Fe_2O_3 in (i) 1 mM AA alone, and mixture of (ii) 4.76 µM DA and 0.95 mM AA, (iii) 9.09 µM DA and 0.91 mM AA, (iv) 13.04 µM DA and 0.87 mM AA, (v) 20.0 µM DA and 0.8 mM AA, (vi) 25.93 µM DA and 0.74 mM AA, and (vii) 28.57 µM DA and 0.71 mM AA in PBS pH 7.0.

In this study, the potential difference of 190 mV between the two analytes is large enough for the determination of one in the presence of the other. However, the electrode appeared weak towards AA detection thus enhancing a negative shift (about 170 mV) in DA signal, with increasing DA

current as DA concentration increases (ii-vii) while AA peaks disappeared completely. The implication of this result is that, there is no possible fouling effect due to AA oxidation intermediates, and the EPPGE-MWCNT-Fe_2O_3 electrode attracted DA strongly leading to enhanced catalysis and fast electron transport towards DA oxidation.

3.7. Real sample analysis: Dopamine drug

The potential applicability of the EPPGE-MWCNT-Fe_2O_3 electrode was tested with a square wave voltammetric assay of dopamine present in a dopamine hydrochloride injection (dopamine content of 200 mg / 5 mL or 40 mg / mL). The concentration found in each dopamine drug (Table 3) agreed closely with the labelled amount, with average recovery (n=5) of 100.6±2.37% at 95% confidence limit. The result proves the suitability of the EPPGE-MWCNT-Fe_2O_3 electrode for DA detection in biological samples.

Table 3. Dopamine content in dopamine hydrochloride injections (40 mg mL^{-1}), n =5 (at 95% confidence limit).

Sample	Concentration found (mg mL^{-1})	Recovery (%)
1	40.6 ± 0.52	101.5 ± 1.30
3	39.9 ± 1.01	99.8 ± 2.53
4	39.5± 0.96	98.7 ± 2.38
2	40.9 ± 1.24	102.2 ± 3.09

4. CONCLUSIONS

The study described the electron transfer properties and electrocatalytic behaviour towards the detection of dopamine using iron oxide nanoparticle (γ-Fe_2O_3) catalysts supported on MWCNTs. We showed that these synthesized γ-Fe_2O_3 nanparticles exhibit comparable electrocatalytic behaviour with their previously-reported electrodeposited forms, but uniquely different in terms of the electrochemical properties. The electrode may be potentially used for the detection of DA in real drug sample analysis.

ACKNOWLEDGEMENTS
We thank the National Research Foundation (NRF) for their support. ASA thanks Obafemi Awolowo University Ile-Ife, Nigeria for a PhD study leave and the University of Pretoria for graduate bursaries.

References

1. I. Ban, M. Drofenik, D. Makovec, *J. Magnetism and Magnetic Materials*, 307 (2006) 250.
2. S. Guo, D. Li, L. Zhang, J. Li, E. Wang, *Biomaterials*, 30 (2009) 1881.

3. R.W. Cornell, U. Schwertmann, The Iron Oxides, VCH, Weinheim, 1996.
4. R.M. Cornell, U. Schwertmann, The Iron Oxides: Structure, Properties, Reactions, Occurrences and Uses, second ed. Wiley-VCH, Weinheim, 2003.
5. K.I. Ozoemena, T. Nyokong, *J. Electroanal. Chem.*, 579 (2005) 283.
6. K.I. Ozoemena, T. Nyokong, *J. Chem. Soc., Dalton Trans.*, (2002) 1806.
7. M. Siswana, K.I. Ozoemena, T. Nyokong, *Talanta*, 69 (2006) 1136.
8. S. Wang, Q. Xu, X. Zhang, G. Liu, *Electrochem. Commun.*, 10 (2008) 411.
9. S.S. Fan, M.G. Chapline, N.R. Franklin, T.W. Tombler, A.M. Cassell, H. Dai, *Science*, 283 (1999) 512.
10. R.R. Moore, C.E. Bank, R.G. Compton, *Analyst*, 129 (2004) 755.
11. A.S. Adekunle, K.I. Ozoemena, *J. Solid State Electrochem.*, 12 (2008) 1325.
12. M. Musameh, J. Wang, A. Merkoci, Y. Lin, *Electrochem. Commun.*, 4 (2002) 743.
13. F.H. Wu, G.C. Zhou, X.W. Wei, *Electrochem. Commun.*, 4 (2002) 690.
14. K.I. Ozoemena, J. Pillay, T. Nyokong, *Electrochem. Commun.*, 8 (2006) 1391.
15. J. Pillay, K.I. Ozoemena, *Electrochim. Acta*, 52 (2007) 3630.
16. K.I. Ozoemena, D. Nkosi, J. Pillay, *Electrochim. Acta* 53 (2008) 2844.
17. R.P. Deo, N.S. Lawrence, J. Wang, *Analyst*, 129 (2004) 1076.
18. A. Salimi, E. Shariffi, A. Noorbakhsh, S. Soltanian, *Biosens. Bioelectron.*, 22 (2007) 3146.
19. T.E Smith. In Devlin, T. M., Ed.; Textbook of Biochemistry with Clinical Correlations; Wiley-Liss: New York, 1992; p 929.
20. M. Velasco, A. Luchsinger, *Am. J. Ther.*, 5 (1998) 37.
21. P. Damier, E.C. Hirsch, Y. Agid, A. M. Graybiel, *Brain*, 122 (1999) 1437.
22. O.L. Lopez, G. Smith, C.C. Meltzer, J.T. Becker, *Neuropsy. Neuropsy. Behav. Neurol.*, 12 (1999) 184.
23. B.J. Venton, R.M. Wightman, *Anal. Chem.*, 75 (2003) 414A.
24. J.A Liu, G. Rinzler, H. Dai, J.H. Hanfer, R.K. Bradley, P.J. Boul, A. Lu, T. Iverson, K. Shelimov, C.B. Huffman, F.R. Macias, Y.S. Shon, T.R. Lee, D.T. Colbert, *Science*, 280 (1998)1253.
25. Y-P. Sun, X-q. Li, J. Cao, W-x. Zang, H. P. Wang, *Advances in Colloid and Interface Science*, 120 (2006) 47.
26. Y-K. Sun, M. Ma, Y. Zhang, N. Gu, *Colloids and Surfaces A: Physicochem.Eng.Aspects*, 245 (2004) 15.
27. S. Qu, H. Yang, D. Ren, S. Kan, G. Zou, D. Li, M. Li, *J. Colloid Interface Sci.*, 215 (1999) 190.
28. G. Carja, Y. Kameshima, K. Okada, *Microporous and Mesoporous Materials*, 115 (2008) 541.
29. K.L. Double, L. Zecca, P. Costi, M. Mauer, C. Griesinger, S. Ito, D. Ben-shachar, G. Bringmann, R.G. Fariello, P. Riederer, M. Gerlach, *J. Neurochem*., 75 (2000) 2583.
30. A.S. Adekunle, B.O. Agboola, J. Pillay, K.I. Ozoemena, *Sens. Actuators B: Chemical*, 148 (2010) 93.
31. S. Singh, R.C. Buchanan, *Mat. Sc. Engnr. C.*, 27 (2007) 551.
32. G.D. Christian, Analytical Chemistry, 6th ed. John Wiley and Sons New York, 2004, p113.
33. S. Shahrokhian, H. R. Zare-Mehrjardi, *Sens. Actuators B Chem.*, 121 (2007) 530.
34. B.N. Chandrashekar1, B.E. Kumara Swamy, M. Pandurangachar, S.S Shankar1, O. Gilbert1, J.G. Manjunatha, B.S., Sherigara, *Int. J. Electrochem. Sci.*, 5 (2010) 578.
35. A. Balamurugan, S. Chen, *Bioelectrochem.*, 54 (2001) 169.
36. Ali A. Ensafi, M. Taei, T. Khayamian, *Int. J. Electrochem. Sci.*, 5 (2010) 116.
37. G. Alarcon-Angeles, B. Pe´rez-Lo´pez, M. Palomar-Pardave, M.T. Ramırez-Silva, S. Alegret, A. Merkoci, *Carbon*, 46 (2008) 898.
38. M. Mazloum-Ardakani, H. Rajabi, H. Beitollahi, B. B. F. Mirjalili, A. Akbari, N. Taghavinia. *Int. J. Electrochem. Sci*., 5 (2010) 147.
39. M.H. Pournaghi-Azar, R. Sabzi, *J. Electroanal. Chem.*, 543 (2003) 115.

40. M.T. Shreenivas, B.E.K. Swamy, U. Chandra, S.S. Shankar, J.G. Manjunatha, B.S. Sherigara, *Int. J. Electrochem. Sci.*, 5 (2010) 774.
41. K.M. Manesh, P. Santosh, A.I. Gopalan, K.P. Lee, *Electroanalysis*, 18 (2006) 894.
42. Z. Galus, Fundamentals of Electrochemical Analysis, Ellis Horwood Press, New York, 1976, p. 313, Ch. 10.
43. H. Razmi, A. Azadbakht, *Electrochim. Acta*, 50 (2005) 2193.
44. H. Razmi, M. Agazadeh, B. Habibi-A. *J. Electroanal. Chem.*, 547 (2003) 25.
45. A.J. Bard, L.R. Faulkner, Electrochemical Methods: Fundamentals and Applications, 2nd Ed, John Wiley & Sons, 2001, Hoboken NJ.
46. X. Cao, L. Luo, Y. Ding, X. Zou, R. Bian, *Sens. Actuator. B Chem.*, 129 (2008) 941.